Supporting Information

Cesium-containing Triple Cation Perovskite Solar Cells: Improved Stability, Reproducibility and High Efficiency

Michael Saliba,[*ad†] Taisuke Matsui,[b†] Ji-Youn Seo,[a] Konrad Domanski,[a] Juan-Pablo Correa-Baena,[c] Mohammad Khaja Nazeeruddin,[d] Shaik M. Zakeeruddin,[a] Wolfgang Tress,[a] Antonio Abate,[a] Anders Hagfeldt,[c] and Michael Grätzel[a]

[a] *Laboratory of Photonics and Interfaces, Institute of Chemical Sciences and Engineering, École Polytechnique Fédérale de Lausanne, Lausanne CH-1015, Switzerland*

[b] *Advanced Research Division, Materials Research Laboratory, Panasonic Corporation, 1006 Kadoma, Kadoma City, Osaka 571-8501, Japan*

[c] *Laboratory of Photomolecular Science (LSPM) École polytechnique fédérale de Lausanne (EPFL), 1015 Lausanne, Switzerland*

[d] *Group for Molecular Engineering of Functional Materials, Institute of Chemical Sciences and Engineering, École Polytechnique Fédérale de Lausanne, Lausanne CH-1015, Switzerland.*

† These authors contributed equally.

*Corresponding author: MS michael.saliba@epfl.ch

Methods

Substrate preparation and Li-doping TiO_2

Nippon Sheet Glass 10 Ω/sq was cleaned by sonication in 2% Hellmanex water solution for 30 min. After rinsing with deionised water and ethanol, the substrates were further cleaned with UV ozone treatment for 15 min. Then, 30 nm TiO_2 compact layer was deposited on FTO via spray pyrolysis at 450 °C from a precursor solution of titanium diisopropoxide bis(acetylacetonate) in anhydrous ethanol. After the spraying, the substrates were left at 450 °C for 45 min and left to cool down to room temperature. Then, a mesoporous TiO_2 layer was deposited by spin coating for 20 s at 4000 rpm with a ramp of 2000 rpm s^{-1}, using a 30 nm particle paste (Dyesol 30 NR-D) diluted in ethanol to achieve 150-200 nm thick layer. After the spin coating, the substrates were dried at 100 °C for 10 min and then sintered again at 450 °C for 30 min under dry air flow.

Li-doping of mesoporous TiO_2, as described elsewhere,[1] is accomplished by spin coating a 0.1 M solution of Li-TFSI in acetonitrile at 3000 rpm for 10 s followed by another sintering step at 450 °C for 30 min. After cooling down to 150 °C the substrates were immediately transferred in a nitrogen atmosphere glove box (MBraun with pressure varying from 5-6 mbar) for depositing the perovskite films.

Perovskite precursor solution and film preparation

The organic cations were purchased from Dyesol; the lead compounds from TCI; CsI from abcr GmbH. The “mixed” perovskite precursor solutions were deposited from a precursor solution containing FAI (1 M), PbI_2 (1.1 M), MABr (0.2 M) and $PbBr_2$ (0.2 M) in anhydrous DMF:DMSO 4:1 (v:v). We note that this composition contains a lead excess as reported elsewhere.[1, 2]

Then CsI, predissolved as a 1.5 M stock solution in DMSO, was added to the mixed perovskite precursor to achieve the desired triple cation composition.

The perovskite solution was spin coated in a two steps program at 1000 and 6000 rpm for 10 and 20 s respectively. During the second step, 100 µL of chlorobenzene was poured on the spinning substrate 5 s prior to the end of the program. Films with Cs-containing perovskite turned dark immediately after spin coating. The substrates were then annealed (usually at 100 °C) for 1 h in a nitrogen filled glove box.

Hole transporting layer and top electrode

After the perovskite annealing, the substrates were cooled down for few minutes and a spiro-OMeTAD (Merck) solution (70 mM in chlorobenzene) was spin coated at 4000 rpm for 20 s. *Spiro*-OMeTAD was doped with bis(trifluoromethylsulfonyl)imide lithium salt (Li-TFSI, Sigma-Aldrich), tris(2-(1H-pyrazol-1-yl)-4-tert-butylpyridine)- cobalt(III) tris(bis(trifluoromethylsulfonyl)imide) (FK209, Dynamo) and 4-tert-Butylpyridine (TBP, Sigma-Aldrich). The molar ratio of additives for spiro-OMeTAD was: 0.5, 0.03 and 3.3 for Li-TFSI, FK209 and TBP respectively.

Finally, 70-80 nm of gold top electrode was thermally evaporated under high vacuum.

Photovoltaic device testing

The solar cells were measured using a 450 W xenon light source (Oriel). The spectral mismatch between AM1.5G and the simulated illumination was reduced by the use of a Schott K113 Tempax filter (Präzisions Glas & Optik GmbH). The light intensity was calibrated with a Si photodiode equipped with an IR-cutoff filter (KG3, Schott), and it was recorded during each measurement. Current-voltage characteristics of the cells were obtained by applying an external voltage bias while measuring the current response with a digital source meter (Keithley 2400). The usual voltage scan rate was at 10 mV s^{-1} (slow) and no device preconditioning, such as light soaking or forward voltage bias applied for long time, was applied before starting the measurement. The starting voltage was determined as the potential at which the cells furnishes 1 mA in forward bias, no equilibration time was used. The cells were masked with a black metal mask (0.16 cm^2) to fix the active area and reduce the influence of the scattered light. The photocurrent density was scaled to 1000 W/m^2.

Aging under maximum power point tracking was carried out on masked devices which were mounted on a temperature controlled plate. The aging was performed under nitrogen atmosphere and 1-sun equivalent illumination provided by an array of white LEDs. The devices were aged by means of keeping them under maximum load under illumination. The maximum power point was updated every 60 s by measuring the current response to a small perturbation in potential. Additionally, a full JV scan was taken every 15 min (at a scan rate of 100 mV s^{-1} starting from forward bias) which was used to extract the displayed parameters for the aging data.

UV–vis measurements were performed on a Varian Cary 5.

Scanning electron microscopy (SEM) was performed on a ZEISS Merlin HR-SEM.

X-ray powder diffractions were recorded on an X'Pert MPD PRO (Panalytical) equipped with a ceramic tube (Cu anode, λ = 1.54060 Å), a secondary graphite (002) monochromator and a RTMS X'Celerator (Panalytical).in an angle range of 2θ = 5° to 60°.

Photoluminescence spectra were obtained with Florolog 322 (Horiba Jobin Ybon Ltd) with the range of wavelength from 620 nm to 850 nm by exciting at 460 nm. The samples were mounted at 60° and the emission recorded at 90° from the incident beam path.

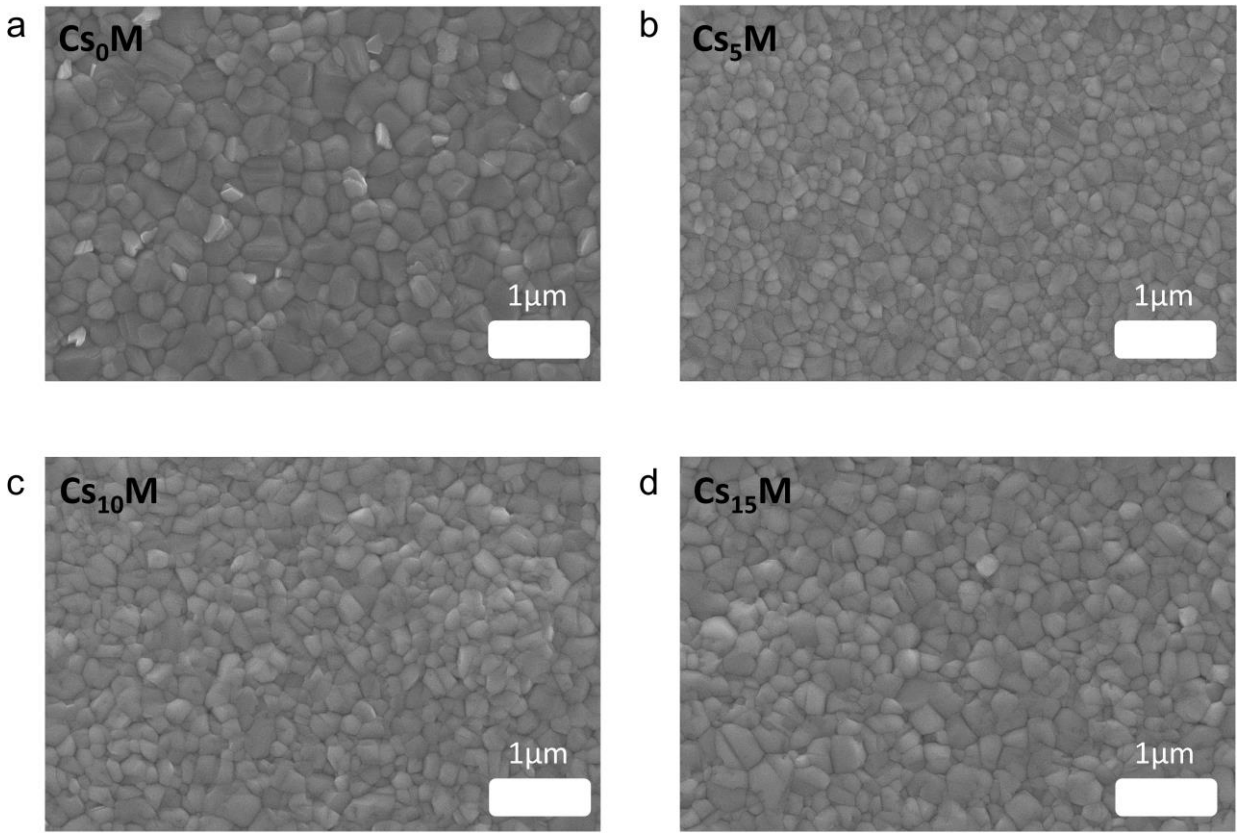

Fig. S1 Top view scanning electron microscope (SEM) images of the Cs_xM series with (a) Cs_0M, (b) Cs_5M, (c) $Cs_{10}M$ and (d) $Cs_{15}M$

Supplementary Note 1

In Fig. S2, we present XRD data with Cs_0M and $Cs_{10}M$ films at different times during the 130 °C aging procedure. As stated in the manuscript the Cs-containing films degrade less quickly than the non-Cs films.

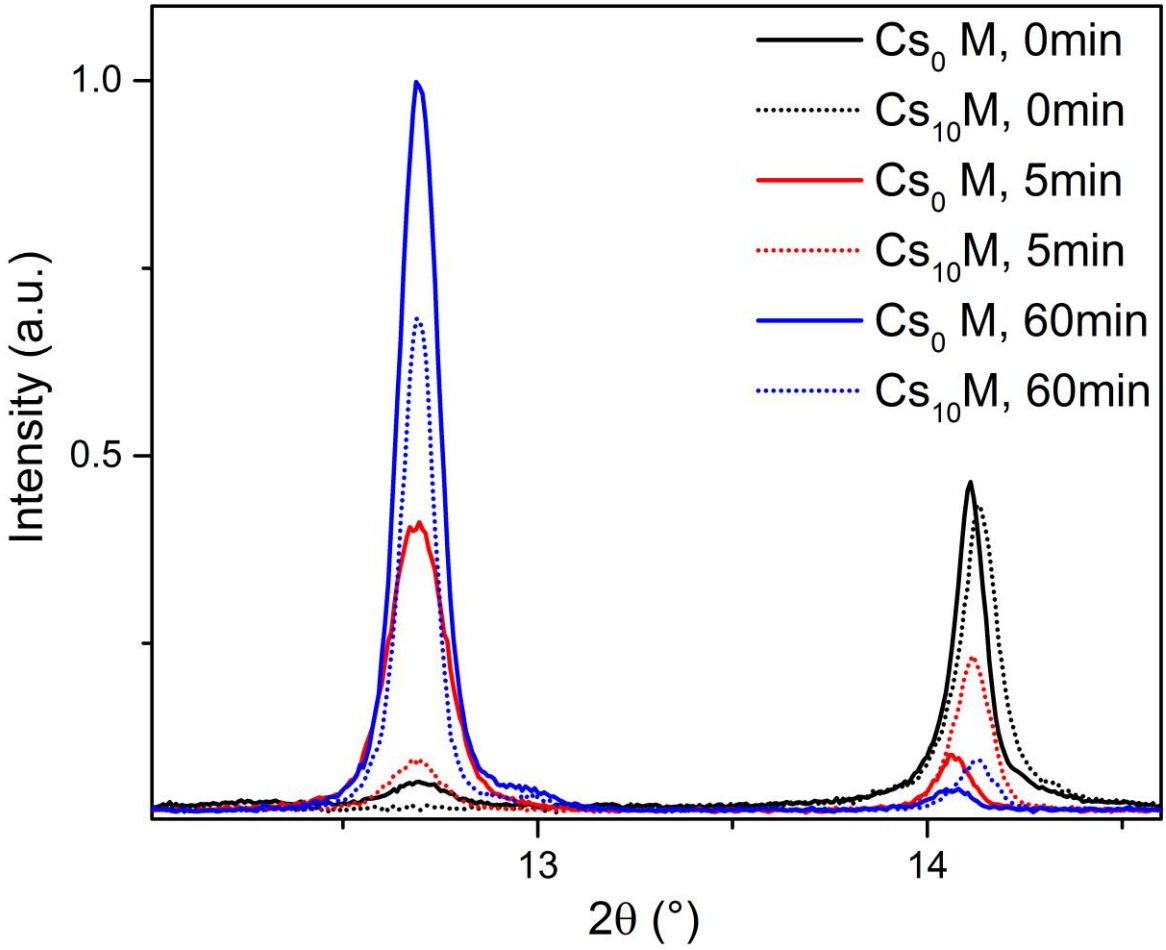

Fig. S2 XRD analysis of Cs_0M (solid curves) and $Cs_{10}M$ (dotted curves) after 0 (black), 5 (red), and 60 min (blue) of heating at 130°C in dry air.

Interestingly, the recent work by McMeekin *et al.* also presents XRD data of the similar $Cs_{0.17}FA_{0.83}Pb(I_{0.6}Br_{0.4})_3$ perovskite which shows almost no thermal degradation after 6 h of aging at 130 °C.[3] In order to relate our result with this finding, we investigated the less bromine containing $Cs_{0.10}FA_{0.90}Pb(I_{0.83}Br_{0.17})_3$, which is the MA-free version of our champion recipe. In Fig. S3, the XRD data reveals that after 4 h at 130 °C, the films start to degrade severely with the clear presence of a PbI_2 peak.

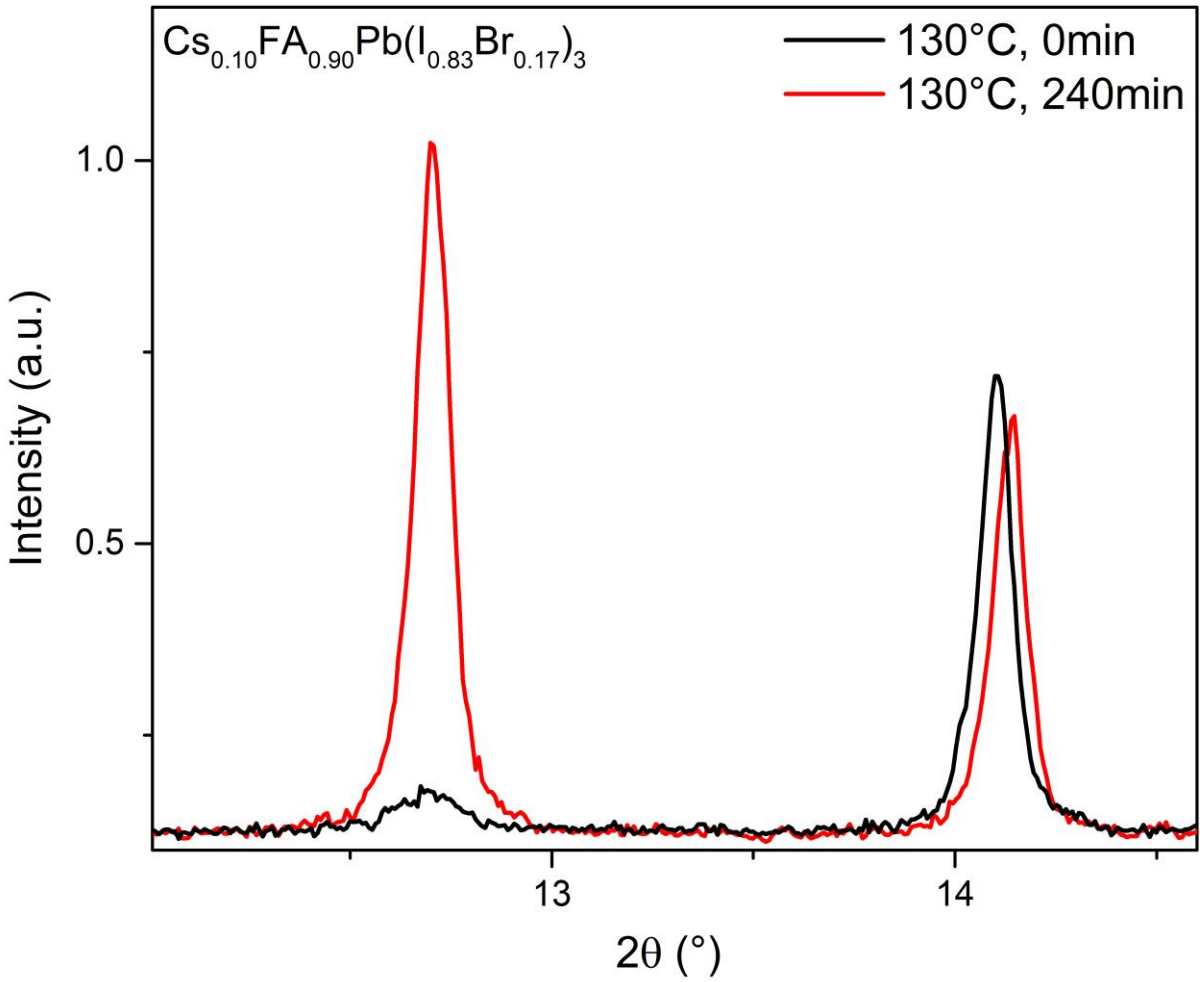

Fig. S3 XRD analysis of $Cs_{0.10}FA_{0.90}Pb(I_{0.83}Br_{0.17})_3$ films (no MA) after 0 (black) and 240 min (red) of heating at 130°C in dry air.

The data agrees well with the fact that the addition of Br stabilizes perovskite films as reported by Misra et al. who show that $MAPbI_3$ degrades rapidly under 100 suns and elevated temperature whereas $MAPbBr_3$ remains stable when treated under these accelerated aging conditions.[4] This is explained with the stronger and shorter Pb-Br bond as compared to Pb-I (due to Br being more electronegative than I). This is also consistent with the data presented by Seok and co-workers who show that $MAPb(I_{1-x}Br_x)_3$ perovskites are significantly more stable against humidity with increasing Br content.[5] Therefore we conclude that Cs increases the thermal stability for a fixed halide ratio and also note that an increased Br content improves the thermal stability irrespective of the cation.

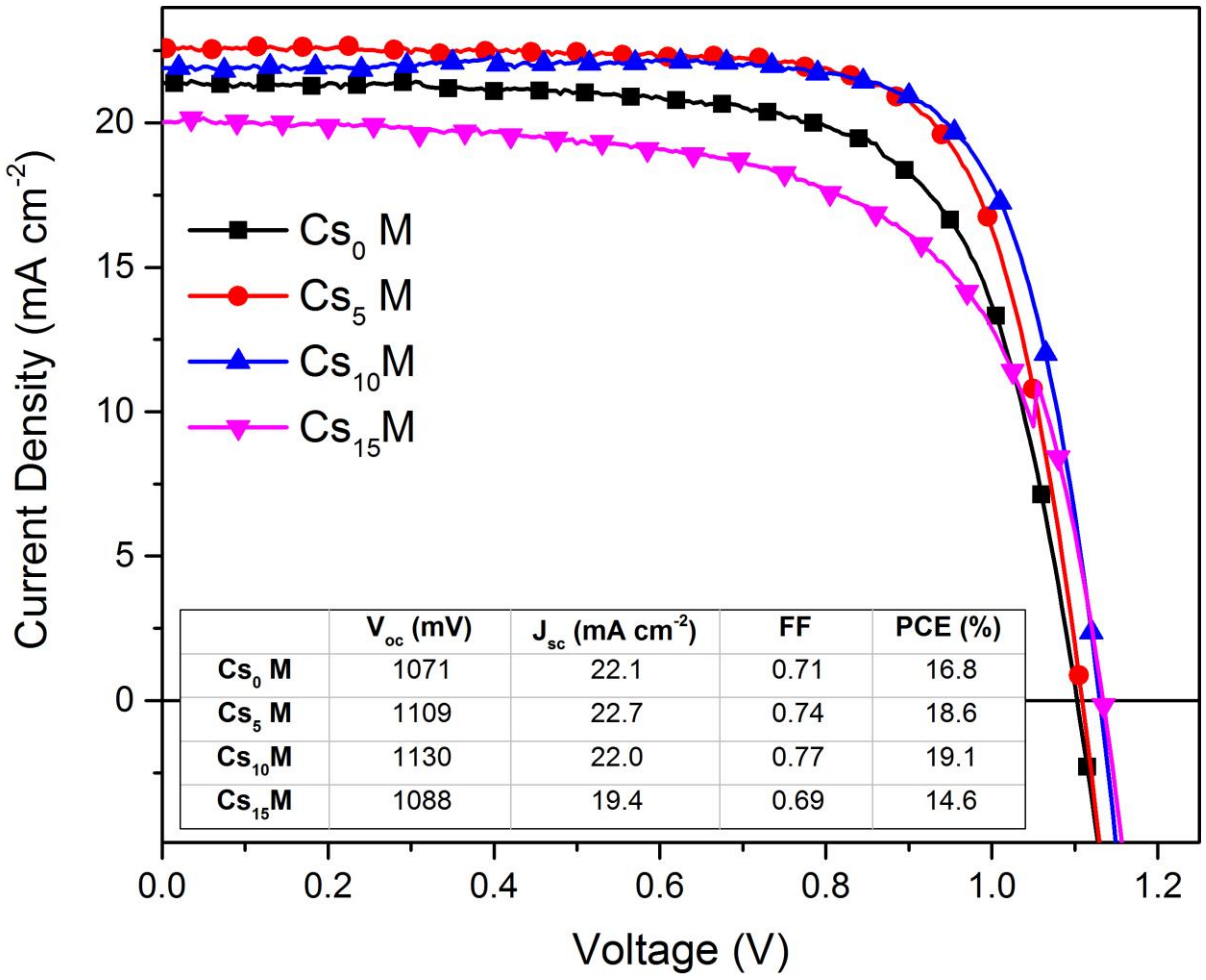

	V_{oc} (mV)	J_{sc} (mA cm^{-2})	FF	PCE (%)
Cs_0 M	1071	22.1	0.71	16.8
Cs_5 M	1109	22.7	0.74	18.6
Cs_{10}M	1130	22.0	0.77	19.1
Cs_{15}M	1088	19.4	0.69	14.6

Fig. S4 JV characteristics for different Cs ratios. (a) JV scans and inset table with short circuit current-density (J_{sc}), open-circuit voltage (V_{oc}), fill factor (FF) and power conversion efficiency (PCE) of the triple cation perovskite compounds C_xM with x = 0, 5, 10, and 15%. More data is presented in Table S1. The voltage scan rate for all scans was 10 mV s^{-1} and no device preconditioning, such as light soaking or forward voltage bias applied for a long time, was applied before starting the measurement.applied for a long time, was applied before starting the measurement.

Table S1 Open-circuit voltage (V_{oc}), short circuit current-density (J_{sc}), fill factor (FF) and power conversion efficiency (PCE) of the triple cation perovskite compounds C_xM

Cs_xM	**V_{oc} (mV)**	**J_{sc} (mA cm^{-2})**	**FF**	**PCE (%)**
15%	1134	20.0	0.64	**14.5**
15%	1088	19.4	0.69	**14.6**
10%	1130	22.0	0.77	**19.1**
10%	1120	21.9	0.76	**18.6**
5%	1095	22.5	0.72	**17.7**
5%	1109	22.7	0.74	**18.6**
0%	1103	21.4	0.70	**16.5**
0%	1071	22.1	0.71	**16.8**

Supplementary Note 2

With three cations present, the parameter space for possible compositions is increased accordingly (especially considering that the halide ratio could be tuned as well). Thus, we look at compositions of the smaller cations, Cs and MA, and their influence on a fixed FA ratio. Consequently, the compositions are of the form $A_xFA_{(1-x)}Pb(Br_{0.17}I_{0.83})_3$ where A = $Cs_yMA_{(100-y)}$. As a first example, we investigated the$Cs_{10}M$ composition where the ratio of Cs:MA:FA is ~10:15:75, i.e. in the above formalism x = 25% and y = 10%. Varying the ratio of Cs:MA with respect to FA helps improving the interplay of the three cations. In Fig. S5 and Table S2, we show a series with a fixed x = 25% where y is varied from 0 (no Cs) to 25% (no MA). We can already observe that the pure MA/FA ratio does not work well for these compositions (with relatively low current densities and fill factors) which is in good agreement with the fact that the optimum for this composition was found to be at ratios of MA:FA of 17:83 instead of 25:75. However, the Cs/FA compound (y = 25%) does not perform significantly better (with higher current densities that are counteracted by lowered voltages). The optimum of this series is at y = 15% where both Cs and MA is present (which coincides closely with the $Cs_{10}M$ composition). Here, the fill factor shows improvement (0.75) and the overall PCE is close to 17% showing that the presence of both Cs and MA is highly relevant. We speculate that the small size of Cs is particular effective at tuning the tolerance factor such that a black phase of FA is stabilized at room temperature. MA, on the other hand, slows down the crystallisation process, which is important for growing defect-free films. In addition, the MA lowers the size discrepancy between Cs and the effective MA/FA cation, which could otherwise lead to a large lattice mismatch. Thus, fine-tuning the ratio of Cs/MA serves to supress the yellow phase of FA perovskite and get defect-free films.

We ascribe this effect to the suppression of yellow phase impurities which, even in small amounts, can hamper charge transport and extraction due to the different energy levels with the black phase perovskite (acting effectively as recombination centres). This is consistent with the device performance where Cs_5M is outperforming Cs_0M due to significantly higher short circuit current and an exceptionally high fill factor of ~0.8, which is a value rarely reached even for the highest performing perovskite solar cells.

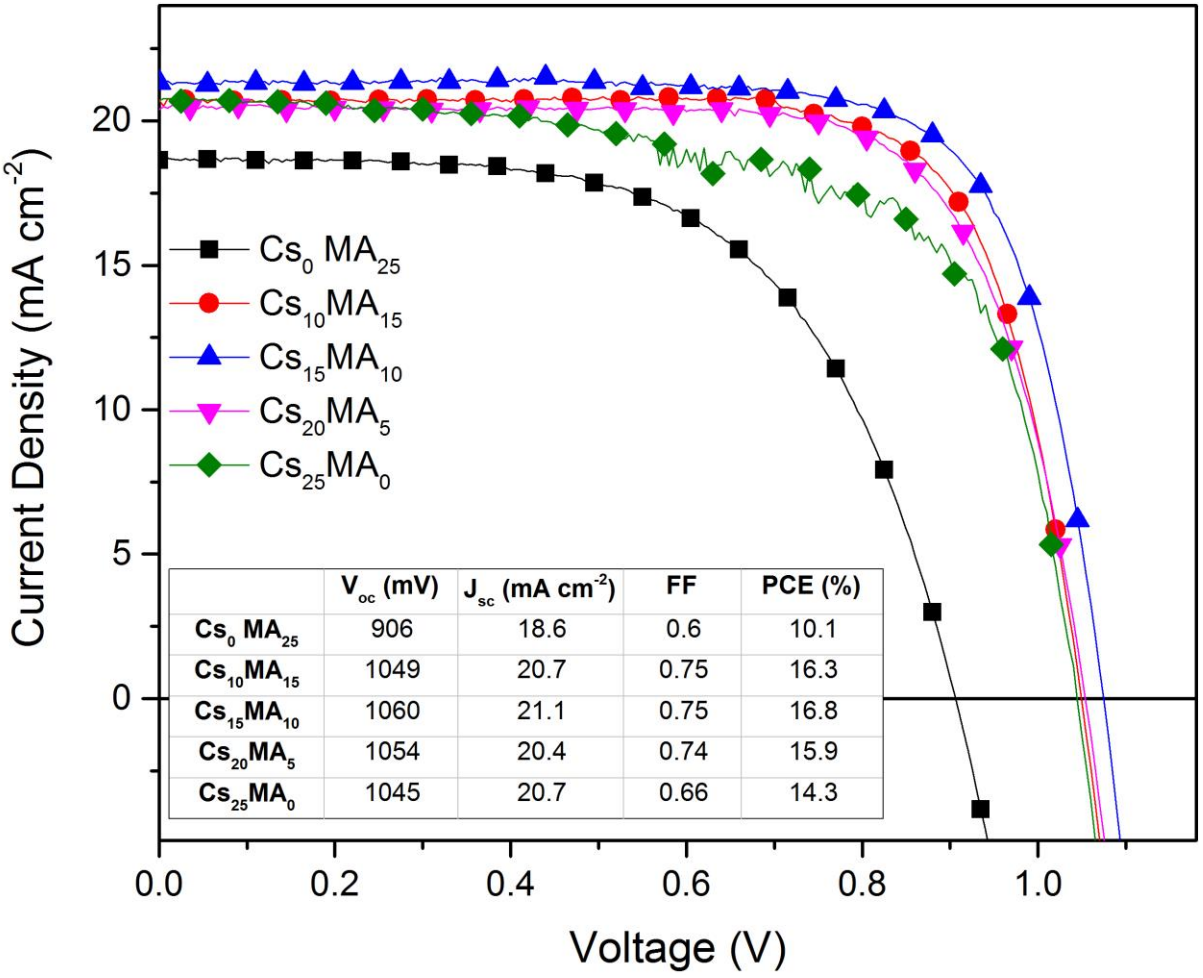

	V_{oc} (mV)	J_{sc} (mA cm^{-2})	FF	PCE (%)
Cs_0MA_{25}	906	18.6	0.6	10.1
$Cs_{10}MA_{15}$	1049	20.7	0.75	16.3
$Cs_{15}MA_{10}$	1060	21.1	0.75	16.8
$Cs_{20}MA_5$	1054	20.4	0.74	15.9
$Cs_{25}MA_0$	1045	20.7	0.66	14.3

Fig. S5 Different Cs:MA:FA ratios. JV scans and inset table with performance parameters for perovskite compounds of the form $A_xFA_{(100-x)}Pb(Br_{0.17}I_{0.83})_3$ where A = $Cs_yMA_{(100-y)}$ with fixed x = 25%, and y = 0, 1, 15, 20, and 25%. More data is presented in Table S2. The voltage scan rate for all scans was 10 mV s^{-1} and no device preconditioning, such as light soaking or forward voltage bias applied for a long time, was applied before starting the measurement.

Table S2 Open-circuit voltage (V_{oc}), short circuit current-density (J_{sc}), fill factor (FF) and power conversion efficiency (PCE) of the triple cation perovskite compounds $A_xFA_{(100-x)}Pb(Br_{0.17}I_{0.83})_3$ where A = $Cs_yMA_{(100-y)}$. y = 0% is a Cs-free perovskite. y = 10% corresponds to $Cs_{10}M$ and y = 25% is an MA-free perovskite.

	y	V_{oc} (mV)	J_{sc} (mA cm^{-2})	FF	PCE (%)
x = 25%	25%	1045	20.7	0.66	**14.3**
	25%	1021	20.9	0.58	**12.4**
	21%	1054	20.4	0.74	**15.9**
	21%	1022	20.7	0.72	**15.2**
	15%	1050	20.9	0.73	**16**
	15%	1060	21.1	0.75	**16.8**
	10%	1076	21.0	0.66	**14.9**
	10%	1049	20.7	0.75	**16.3**
	5%	913	17.9	0.52	**8.5**
	0%	906	18.6	0.60	**10.1**

Table S3 “Bad batch”. Open-circuit voltage (V_{oc}), short circuit current-density (J_{sc}), fill factor (FF) and power conversion efficiency (PCE) of the triple cation perovskite compounds $A_xFA_{(100-x)}Pb(Br_{0.17}I_{0.83})_3$ where A = $Cs_yMA_{(100-y)}$ with x = 17%. y = 0% corresponds to Cs_0M, i.e. it contains only MA/FA and no Cs. y = 17% contains only Cs/FA and no MA.

y	V_{oc} (mV)	J_{sc} (mA cm^{-2})	FF	PCE (%)
17%	1061	20.4	0.73	**15.8**
17%	1059	20.5	0.71	**15.4**
14%	1105	20.4	0.71	**16**
14%	1083	20.9	0.72	**16.3**
10%	1078	20.9	0.72	**16.2**
10%	1071	21.0	0.72	**16.2**
5%	1044	19.4	0.72	**14.6**
5%	1092	20.3	0.7	**15.5**
0%	1079	18.8	0.66	**13.4**
0%	1034	18.9	0.66	**12.9**

Table S4 Open-circuit voltage (V_{oc}), short circuit current-density (J_{sc}), fill factor (FF) and power conversion efficiency (PCE) of the best performing Cs_5M in Fig. 5a. The curves were recorded at a scan rate of 10 mV s^{-1} from forward bias (FB) to the short circuit condition (SC), and the other way around. Devices were masked with a metal aperture of 0.16 cm^2 to define the active area. No device preconditioning, such as light soaking or forward voltage bias applied for long time, was applied before starting the measurement.

Scan direction	**J_{sc} (mA cm^{-2})**	**V_{oc} (mV)**	**FF**	**PCE (%)**
FB to SC	23.5	1147	0.785	**21.17**
SC to FB	23.5	1158	0.746	**20.32**

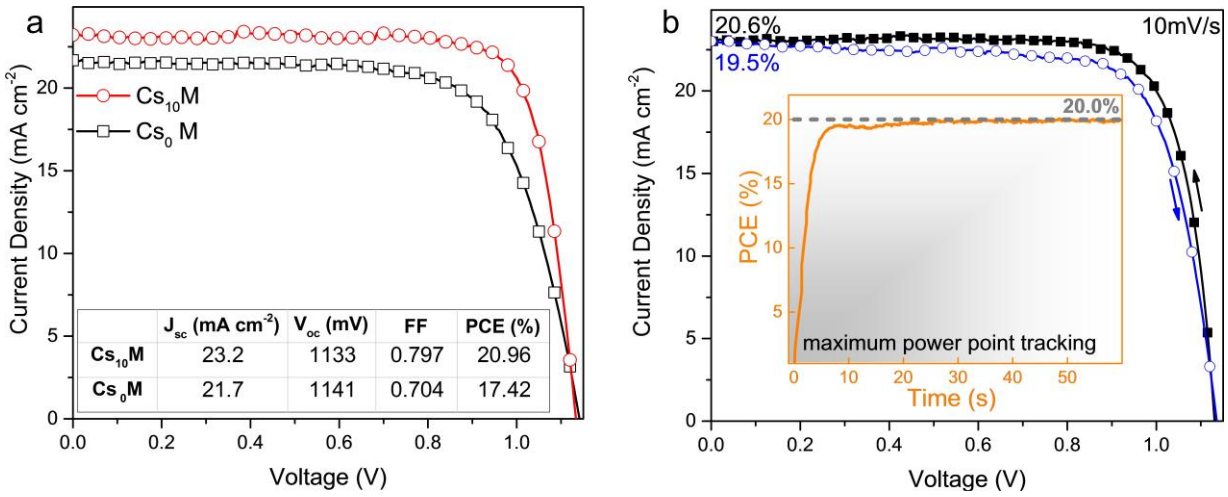

Fig. S6 JV and stability characteristics (a) Current-voltage scans for the best performing $Cs_{10}M$ device and the Cs_0M control (from the same batch) alongside the extracted performance parameters in the table (inset) showing PCEs close to 21%.The voltage scan rate for all scans was 10 mV s^{-1} and no device preconditioning, such as light soaking or forward voltage bias applied for a long time, was applied before starting the measurement. The full hysteresis loop is reported in Table S5. The short circuit current is in agreement with the EQE measurement in Fig S7. (b) High performing Cs_5M device. The scan from forward bias to short circuit gives 20.6% and the reverse scan shows 19.5%. The full hysteresis loop parameters are reported in Table S6. The inset shows the power output under maximum power point tracking for 60 s, starting from forward bias and resulting in a stabilized power output of 20% (reached at 900 mV).

Table S5 Device parameters of the JV curves in Fig. S6a.

perovskite	Scan direction	J_{sc} (mA cm^{-2})	V_{oc} (mV)	FF	PCE (%)
$Cs_{10}M$	FB to SC	23.2	1132	0.797	**20.96**
	SC to FB	23.3	1146	0.747	**19.95**
Cs_0M	FB to SC	21.7	1141	0.704	**17.42**
	SC to FB	21.7	1115	0.716	**17.31**

Table S6 Device parameters of the JV curves in Fig. S6b.

Scan direction	J_{sc} (mA cm^{-2})	V_{oc} (mV)	FF	PCE (%)
FB to SC	23.1	1131	0.790	**20.6**
SC to FB	23.0	1136	0.745	**19.5**

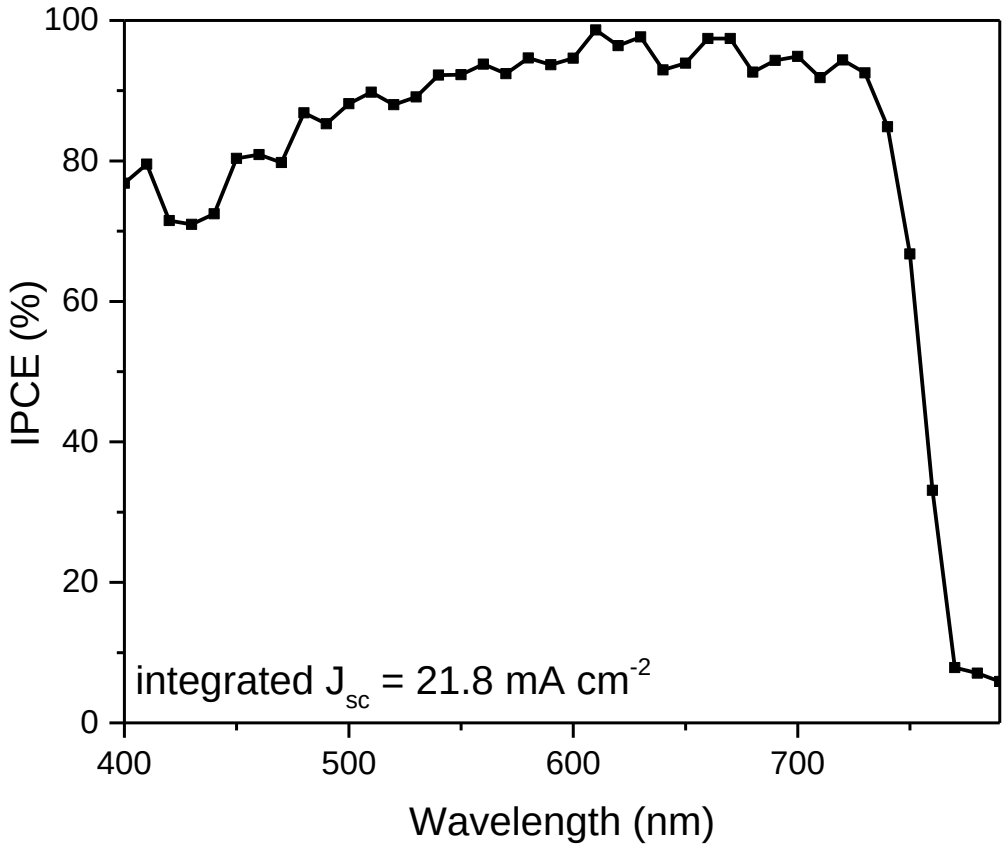

Fig. S7 External quantum efficiency of the device in Fig. S6a. The integrated short circuit current density of 21.8 mA cm^{-2} follows the JV scans from the solar simulator.

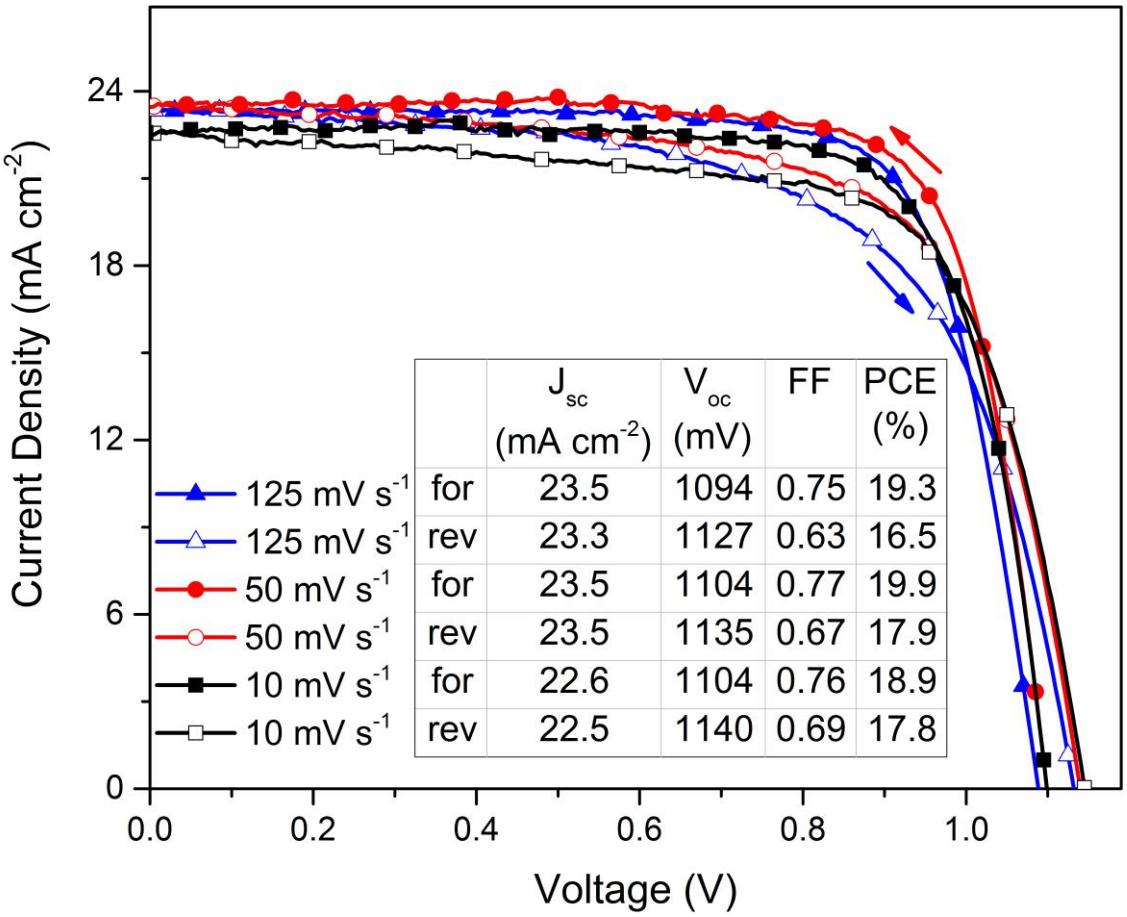

Fig. S8 Cs_5M device measured at different scan rates (10, 50 and 125 mV s^{-1}). The solid symbols denote scans from forward bias (FB) to the short circuit condition (SC) (abbreviated as “for”). The reverse direction (open symbols) is referred to as “rev”. The inset shows the corresponding device parameters. No device preconditioning, such as light soaking or forward voltage bias applied for long time, was applied before starting the measurement.

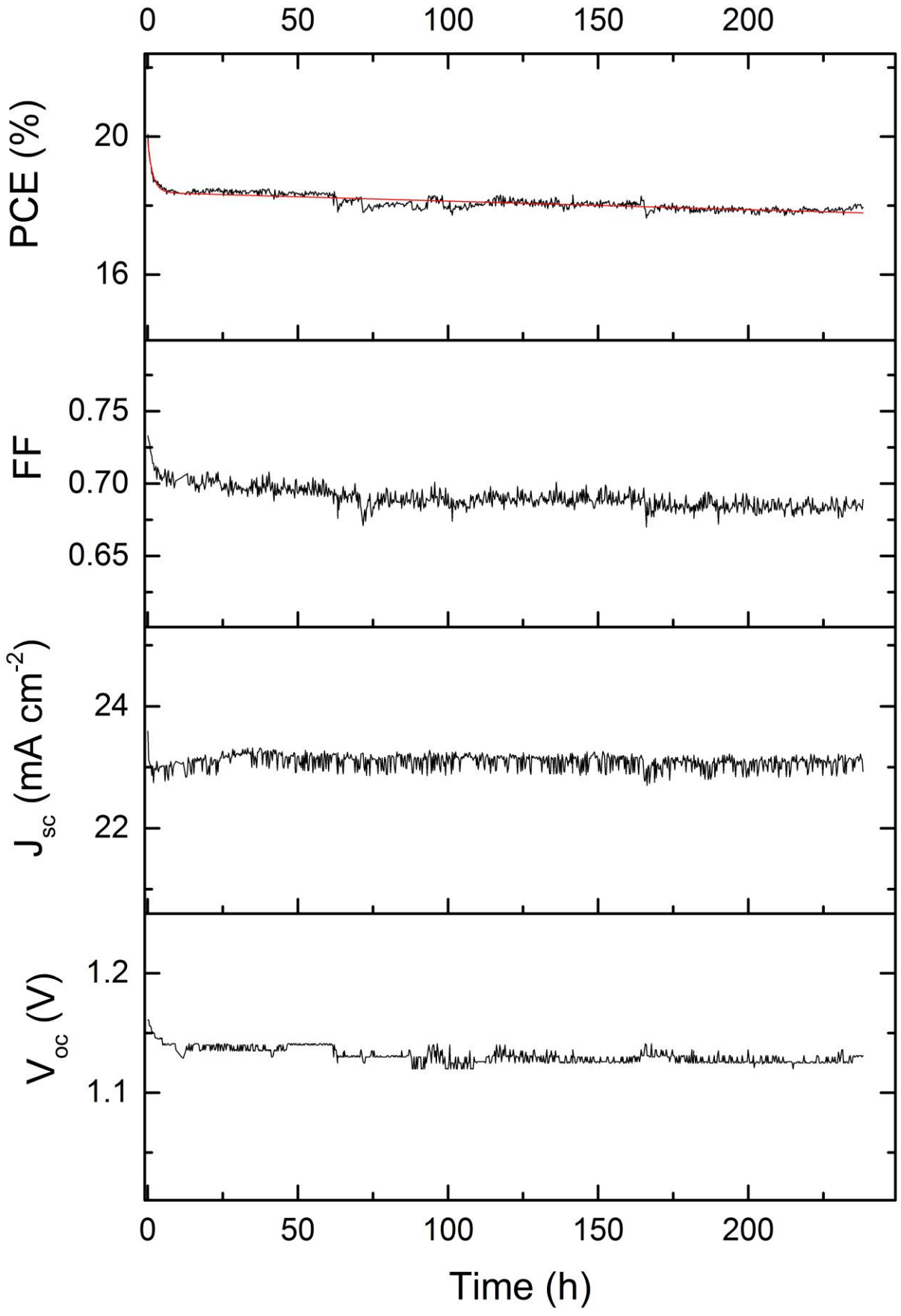
0
50
100
150
200
PCE (%)
20
16
FF
0.75
0.70
0.65
J_sc (mA cm^-2)
24
22
V_oc (V)
1.2
1.1
0
50
100
150
200
Time (h)

Fig. S9 PCE, FF, J_{sc} and V_{oc} for long-term aging of a high performance Cs_5M device (with a starting PCE of 20%) in nitrogen atmosphere at room temperature under constant illumination and maximum power point tracking. The maximum power point was updated every 60 s by measuring the current response to a small perturbation in potential. A JV scan was taken periodically to extract the device parameters. This aging test resembles sealed devices under realistic operational conditions (as opposed to "shelf stability" of devices kept in a dry atmosphere in the dark). The red curve for the PCE is a biexponential fit as reported in Table S7. The long-lived component (t2*ln2) is 5032 h which is one of the most promising stability values reported for high efficiency perovskite solar cells.

Table S7 Fitting parameters of the PCE curve in Fig. S8 for a biexponential equation of the form y = A1*exp(-x/t1) + A2*exp(-x/t2) + y0.

Adj. R-Square	0.764	
	Value	**Standard Error**
y0	0	0
A1	1.51311	0.08411
t1	1.68658	0.14526
A2	18.38261	0.00868
t2	7258.93022	179.66342

Fast half-life constant = t1*ln2 = 1.2 h
Slow half-life constant = t2*ln2 = 5032 h

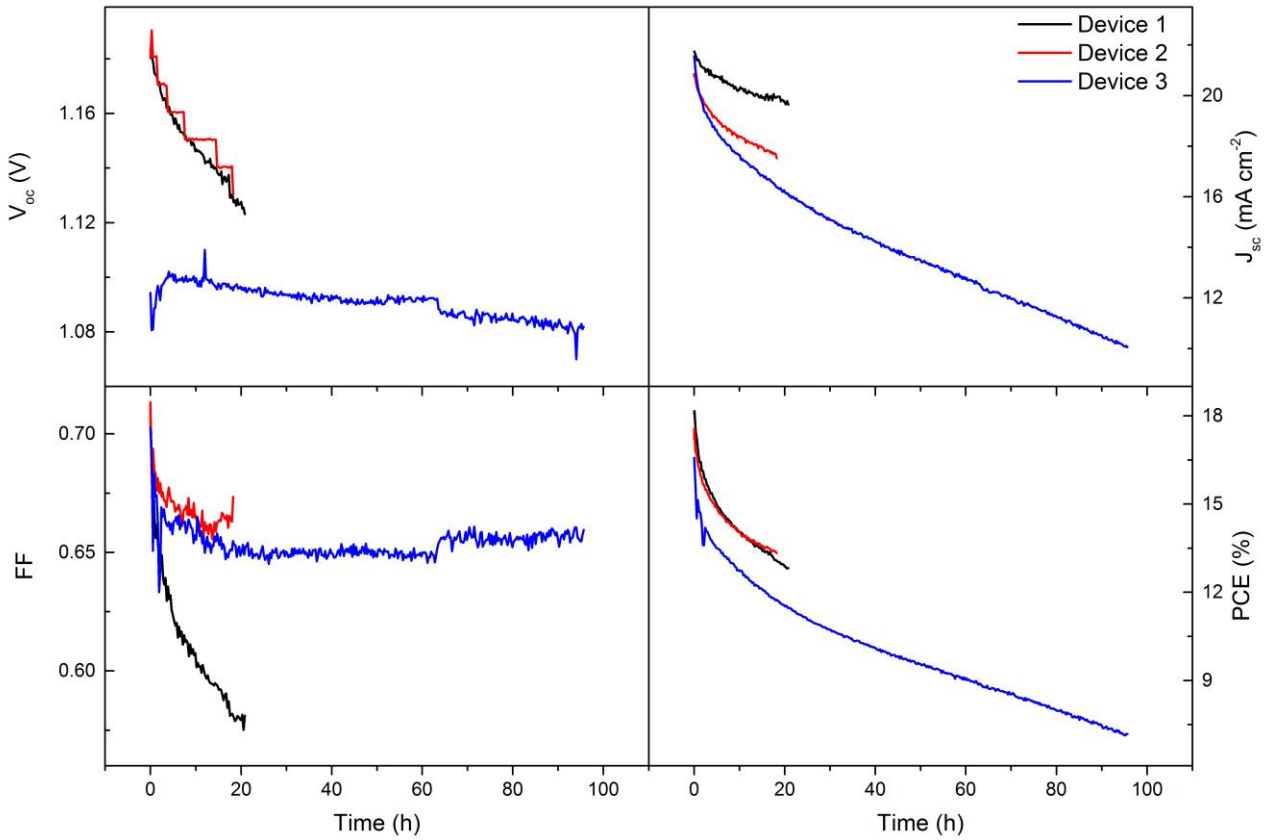

Fig. S10 Device parameters for long-term aging for 3 different high performing Cs_0M control devices in nitrogen atmosphere at room temperature under constant illumination and maximum power point tracking. This aging test resembles sealed devices under realistic operational conditions (as opposed to “shelf stability” of devices kept in a dry atmosphere in the dark). The current decreases significantly for all three control devices.

References

1. F. Giordano, A. Abate, J. P. Correa Baena, M. Saliba, T. Matsui, S. H. Im, S. M. Zakeeruddin, M. K. Nazeeruddin, A. Hagfeldt and M. Graetzel, *Nat Commun*, 2016, **7**, 10379.
2. D. Bi, W. Tress, M. I. Dar, P. Gao, J. Luo, C. Renevier, K. Schenk, A. Abate, F. Giordano, J. P. Correa Baena, J. D. Decoppet, S. M. Zakeeruddin, M. K. Nazeeruddin, M. Gratzel and A. Hagfeldt, *Sci Adv*, 2016, **2**, e1501170.
3. D. P. McMeekin, G. Sadoughi, W. Rehman, G. E. Eperon, M. Saliba, M. T. Horantner, A. Haghighirad, N. Sakai, L. Korte, B. Rech, M. B. Johnston, L. M. Herz and H. J. Snaith, *Science*, 2016, **351**, 151-155.
4. R. K. Misra, S. Aharon, B. Li, D. Mogilyansky, I. Visoly-Fisher, L. Etgar and E. A. Katz, *J Phys Chem Lett*, 2015, **6**, 326-330.
5. J. H. Noh, S. H. Im, J. H. Heo, T. N. Mandal and S. I. Seok, *Nano Lett*, 2013, **13**, 1764-1769.